Jurnal Kejuruteraan 33(2) 2021: 257-264
https://doi.org/10.17576/jkukm-2021-33(2)-11

Experimental and Numerical Analyses of Wind-Induced Noise in Two-Way Radios

Wan Masrurah Hairudin, Ummi Masyitah Mohd Fisol & Norilmi Amilia Ismail
School of Aerospace Engineering,
Engineering Campus, Universiti Sains Malaysia, Malaysia

**Corresponding author: aenorilmi@usm.my*

Received 03 March 2020, Received in revised form 03 September 2020
Accepted 01 October 2020, Available online 30 May 2021

ABSTRACT

The generation of wind noise of entrance microphone cavities owing to turbulent airflow is an inherent problem with radio telecommunication systems, such as two-way radios. It will lead to a pressure fluctuation which is highly unpleasant and would degrade a two-way radio communication. This research aims to understand the relationship between noise level and the flow structure of the different parameters to the occurrence of noise during communication using a two-way radio device. A noise measurement is conducted to analyse the sound pressure level (SPL) within a cavity, in which computational fluid dynamic(CFD) is used to investigate the flow behaviour on the various effects of cavity positions at P1, P2, P3, P4, and P5 and wind velocities of 0.75 m/s, 1.49 m/s, 2.24 m/s, 2.99 m/s and 3.75 m/s which corresponding to Reynolds number (Re) of 8694, 17389, 26083, 34777, and 43471 respectively. CFD result showed the presence of separation of the shear layer, the development of vortex shedding, the recirculation region and vorticity were present inside the edges of the cavity. SPL increased with an increase in wind velocity and, the cavity distance of P4. In the cavity position of P5, SPL is decreased due to the wind velocity exceeding the maximum level of a wind tunnel. Therefore, the cavity position of P5 is suitable for reducing wind noise. These parameters are significant for improving the design of two-way radio to reduce the noise during outdoor communication.

Keywords: Wind-induced noise; CFD; Sound pressure level (SPL); microphone cavity; two-way radio; cavity

INTRODUCTION

A two-way radio is a radio that can receive and transmit radio signals. It has been used to eliminate obscured communications at large sites, such as the hospitals, security, military installations, oil rig platform. However, the issue of unclear audio with background noise is evident because of exposure to windy conditions. Wind flow affects the quality of the signal. The received signal which, is unclear because of the noise induced by the wind creates a signal which may be equal to or greater than the voice of the user.

In general, wind-induced noise can be generated from the hydrodynamic instability of the airflow over the cavity. Wind flows across an opening cavity produce separating vortices and elevated the noise. This noise is also referred to as the aero-acoustic phenomenon (Proskurov, 2017). This condition can cause significant noise signal disruption and damage to the structural integrity of the device system (Kook et al. 2002).

A two-way radio has a flow-receiving cavity, hits the diaphragm and microphone, and then converts the flow to a signal. Figure 1 shows the flow cavity noise mechanism Air that flows across the open cavities, creates the vortices. These vortices flow until they reach and impact the other end (i.e point B), thereby forming strong acoustics that propagates in the environment. Noise reaches point A, where it stimulates the formation of new vortexes which will repeat the process and generates even more noise.

The wind-induced noise phenomenon is produced by the wind that impinges on the sharp edges of the microphone cavity. The current literature has shown that mechanics of this have yet to be fully understood. Previously studies have introduced the empirical formula and field measurement to determine the wind noise (Morgan et al. 1992; Zhao et al. 2017). Morgan et al. (1992) explained that the interaction of turbulent wind flow impinges upon microphone surfaces, which is the primary source of wind-induced noise. They conducted an empirical study in a windy environment, using bare and shielded microphones at different diameters and porosities. Wang et al. (2012) proposed a new technique using two shielded microphones to distinguish noise from the acoustic signal by utilizing the incoherent output power. Their results showed that this technique could estimate a reduction in wind noise around 3 to 5 dB. They also examined and characterized the wind-induced noise in an anechoic wind tunnel under different windshield shapes. Zhao et al. (2018) used other method such as microphone array, to mitigate wind noise using a microphone array. The experimental results showed that the proposed method could reduce wind noise by approximaely 10 dB at a frequency range of 500 Hz. The majority of the preceding studies have considerably focused on outdoor microphone and indoor

wind noise measurements. However, a minimal reference was noted of the effect of a turbulent flow behaviour that impinges on the surface of microphone cavity.

Several studies have used wind tunnel testing and computational fluid dynamics (CFD) simulation to perform wind-induced noise in a two-way radio. Fisol et al. (2013) conducted the wind tunnel test and used sound level measurement, to investigate the relationship between wind speed and noise level. Their study showed a higher wind speed at an angle of attack of 15º when the noise level increased. Hashim et al. (2013) investigated the sound quality of the two-way radio by measuring the effect of angle orientation, wind speed and the intelligibility of the received speech signal by threshold hearing level. The results showed that the angle leads to the worst noise effect induced by wind being at 90° to the leading edge, which also shows the highest of sound pressure level.

Only a few studies have used numerical simulation to analyze the flow behaviour. Yow et al. (2013) included a numerical solution for evaluating the experimental study to minimize the problem of wind-induced noise that exists in electronic device outdoors. The result showed good agreement in vector speed, profile, and vortex core contour between simulation and experimental method. They also agreed if the next researcher to use a Rossiter's formula in wind noise. Hairudin et al. (2020) investigated the relationship between the cavity and the wind source. The results concluded that position the furthest position from the wind source is a suitable position to reduce the wind-induced noise produced.

Saw et al. (2018) invented a slim tunnel wind port to be used for a communication device. They proposed a small tunnel at the above of the microphone cavity to reduce the noise by the wind. The small tunnel disrupts the turbulence formation, which causes discrete vortices when the wind moves across the device surface. Therefore, there would also be minimal turbulence and wind-induced noise. Qualitative method, such as flow visualization and measurement, can be used to obtain a better understanding of the noise phenomena inside the cavity. Experiments, however, are expensive and require complex image processing to generate a good image for analysis. Alternatively, a simulation approach may be used to analyze the flow structure to reduce the wind induced noise.

CFD is a simulation method software for predicting the flow field and noise inside a cavity. Liu et al. (2012) used a hybrid CFD scheme; ANSYS CFD (Fluent) and ACTRAN to investigate development of vortex shedding and the acoustic waves within whistle. The Helmholtz resonator was used to analyze the result of the measurement. Das and Kurian (2013) used ANSYS Fluent to perform a 2D and 3D cavity of varying length to width (L/W). The turbulence model k-epsilon (RANS) was used to represent the unsteady flow field, and self-sustaining pressure oscillations inside a cavity. The simulation results showed that the flow field and acoustic depend on the cavity width of the cavity. Ravulapati et al. (2014) performed a CFD study to understand the formation of vortices and separation bubbles inside the square and cylindrical cavity at different Reynolds numbers (Re). The test results showed that the separation of the bubbles occurred at the upper and bottom corner cavities. It also showed the results in the cylindrical cavity, specifically at higher Reynolds number. Zhang et al. (2010) simulated the cavity flow noise using large eddy simulation (LES) and FW-H acoustic analogy. The pressure fluctuation inside the cavity was investigated and compared to experimental results. The findings showed that the comparisons made are accurate. Note that numerical studies on cavity within two-way radio have yet to fully explored flow behaviour and noise level within small cavities with low wind speed.

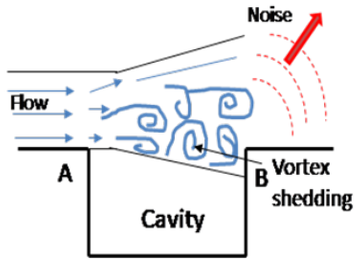

FIGURE 1. Wind-induced noise mechanism inside a cavity

This research aims is to analyse the flow behavior and sound pressure level (SPL) produced within a small cavity of two-way radio in the wind tunnel and CFD simulation. The current study mainly contributes to the literature on the impact of wind induced noise on two way radios. Firstly, this study discusses the important relationship between cavity distance and the source of the noise. Secondly, the current authors understand how vortex formation occurred inside the cavity.

GOVERNING EQUATIONS

The governing equations describing the fluid flow are conservation of mass, momentum and energy. The conservation of mass of incompressible Navier – Stokes equations can be written in a continuity equation as follows:

$$\frac{\partial u}{\partial x}+\frac{\partial v}{\partial y}=0 \tag{1}$$

The conservation of momentum in x and y direction are described as follows:

$$u\frac{\partial u}{\partial x}+v\frac{\partial u}{\partial y}=-\frac{\partial p}{\partial x}+\frac{1}{R_e}\left(\frac{\partial^2 u}{\partial x^2}+\frac{\partial^2 u}{\partial y^2}\right) \tag{2}$$

$$u\frac{\partial v}{\partial x}+v\frac{\partial v}{\partial y}=-\frac{\partial p}{\partial y}+\frac{1}{R_e}\left(\frac{\partial^2 v}{\partial y^2}+\frac{\partial^2 v}{\partial y^2}\right) \tag{3}$$

Where, u and y are the velocity components in the x and y -directions, respectively, p is the pressure, $R_e = \frac{uL}{\nu}$ is the Reynolds number, and υ is the dynamic viscosity of the fluid inside the cavity.

The total energy equation (E_t) is given as follows:

$$\frac{\partial(E_t)}{\partial t}+\frac{\partial(uE_t)}{\partial x}+\frac{\partial(uE_t)}{\partial y}=-\frac{\partial(up)}{dx}+\frac{\partial(\upsilon p)}{dy}+$$
$$\frac{1}{R_{e_t}}\left[\frac{\partial}{\partial x}\left(u\tau_{xx}+u\tau_{xy}\right)+\frac{\delta}{\partial y}\left(u\tau_{xy}+\upsilon\tau_{yy}\right)\right]-\frac{1}{R_{e_f}Pr_r}\left[\frac{\partial q_x}{\partial x}+\frac{\partial q_y}{\partial y}\right] \quad (4)$$

METHODOLOGY

CAVITY GEOMETRY

Figure 2 shows a schematic a rectangular cavity model. Cavities can be classified based according to ratio of length to depth ratio (L/D), where L is the length and D is the depth of the cavity. There are three types of cavities; 'open' if L/D < 10, 'closed' if L/D >13 and transitional for $10 \leq L/D \leq 13$ (Sridhar, 2012). The rectangular cavity is designed to ensure an open cavity flow. The length to depth ratio *(L/D)* is 1.4, with the dimensions of L (0.014m) and D (0.01m), respectively. Figure 3 shows the five cavity position starting from P1 (0.01m), P2 (0.044m), P3 (0.078m), P4 (0.112m) and P5 (0.146m). The distance of each cavity is based on the length of the two-way radio.

COMPUTATIONAL FLUID DYNAMIC (CFD)

A two-dimensional (2D) geometry airflow over the cavity is simulated using the ANSYS FLUENT CFD software. The inlet flow conditions were set as U = 0.75 m/s, 1.49 m/s, 2.24 m/s, 2.99m/s, and 3.75 m/s which corresponding to the Reynolds numbers of 8694, 17389, 26083, 34777, and 43471, respectively. Wind speed is based on the dynamic similarity of Reynolds number of 8694, 17389, 26083, 34777 and 43471 between the two-way radio and fabricated specimen. In the Reynolds Average Navier Stokes (RANS), the k-ε turbulence model was used to describe the transient flow field and turbulence characteristics. This model was chosen because it has an advantage for outdoor airflow and good performance for unsteady oscillation outdoor airflow simulation (Mishra et al. 2018). Outlet and upper wall boundary condition are selected as pressure far field. Pressure based approach was selected for incompressible low-speed flows, where the air density is assumed constant throughout the simulation. No-slip wall boundary condition is used for cavity wall. A semi-implicit method for pressure-linked equations (SIMPLE) algorithm of the pressure-velocity coupling was selected to solve the governing equations. A time step of $1e^{-3}$ second was used in the computation. Second-order implicit method and second-order upwind (space discretization) are chosen for the time resolution with 20 iterations for each time step. A total of 211,795 quadrilateral element numbers were created. Figure 4 shows a 2D unstructured mesh with uniform quad/tri meshing method of 0.001m in element size and 1000 division of edge sizing. Tables 1 summarized the simulation parameters.

TABLE 1. Simulation parameters of the rectangular cavity

Simulation parameters	Value
Air density, ρ (kg/m^3)	1.225
Kinematic viscosity, υ (kg/m.s)	1.7×10^{-5}
Pressure, P (Pa)	101,325
Time step size (s)	0.001

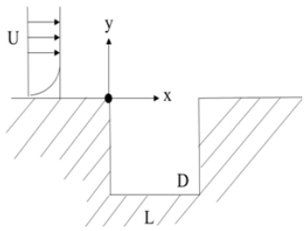

FIGURE 2. The schematic diagram of the cavity

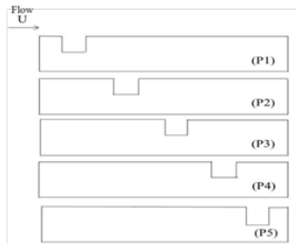

FIGURE 3. The cavity position

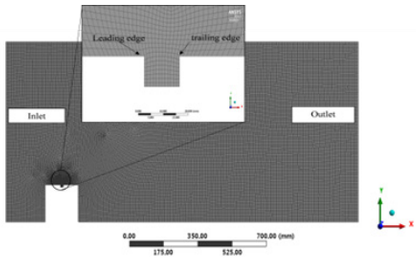

FIGURE 4: The unstructured mesh

SOUND MEASUREMENT

The experiment was conducted in an open-loop wind tunnel in the School of Aerospace Engineering, USM. The open-loop wind tunnel has a 0.32 m (width) x 0.35 m (height) and 0.3m (length) test section and can provide a maximum achievable speed up to 11 m/s with a freestream turbulence intensity of 0.1%. The cavity model is fabricated by using Perspex with a dimension of 0.15 m (height) x 0.291 m

(length) x 0.17 m (width), as shown in figure 5(a). The fabricated model has five holes on the top, which represented as cavities. The wind velocities are measured by using hot-wire anemometer. The basic of the sound measurement, in this case, is three steps. Firstly, the sound measurement started with a background noise. Secondly, the effect of SPL on the different cavity position and wind velocities were measured.

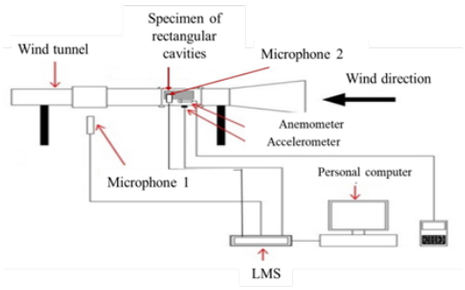

FIGURE 5. The schematic diagram of the test setup.

RESULT AND DISCUSSION

EXPERIMENTAL RESULT: BACKGROUND NOISE

Figure 6 shows the Fast Fourier transform (FFT) graph of background noise and wind noise of the cavity model. According to this figure 6 (a) and 6(b), the amplitude sound pressure (Pa) of the background noise is 0.02 Pa which corresponds to 60 dB; meanwhile, the wind noise graph shows the value of 0.07 Pa corresponding to 70.8 dB. It also shows that the peak noise level is around below 500 Hz, 787.5 Hz and as well as at 4 kHz. The test showed that wind noise shows a higher sound pressure level compared with the background noise level. The background noise in a wind-tunnel must be lower at least 10 dB than with a cavity model, as stated by Pascioni et al. (2014) and Kucukosman et al. (2018).

EXPERIMENTAL RESULT: COMPARISON BASELINE (WITHOUT) AND WITH CAVITY

EFFECT OF WIND VELOCITY AND CAVITY POSITION

Figure 7 shows sound pressure against frequency at different wind velocity with varied cavity position of P1, P2, P3, P4 and P5. This figures showed that the wind-induced noise occurs at a low frequency of 24 Hz. Figure 8(a) showed that sound pressure (Pa) is increased with the increase of wind velocity from 0.75 m/s to 2.99 m/s. However, the sound pressure (Pa) at 3.75 m/s is slightly reduced at the cavity position of P5. Evidently, noise level increased with increasing the wind speed, as determines by Zhang et al. (2010). However, the noise level is reduced when the cavity distance is far from the wind source. It is due to the wind velocity has reached the maximum level of the wind tunnel.

TABLE 2. Summary of experimental result

Reynold numbers	Velocity (m/s)	Sound Pressure (Pa)				
		P1	P2	P3	P4	P5
8694	0.75	0.022	0.020	0.027	0.039	0.044
17389	1.49	0.024	0.024	0.027	0.031	0.052
26083	2.24	0.027	0.021	0.023	0.034	0.060
34777	2.99	0.028	0.026	0.027	0.038	0.055
43471	3.75	0.025	0.037	0.027	0.029	0.071

NUMERICAL SIMULATION RESULT

EFFECT OF CAVITY POSITION

Figure 8 shows the velocity contour for Reynold number of 43471 and the following flow phenomena are observed in the periodic cavity flow. Firstly, free stream is separated inside the cavity and concentrated at the leading edge wall. Secondly, flow separation impinges on the trailing edge wall. Thereafter, it produces a shear layer that reattaches with the flow inside the cavity. The vortex is observed at the upstream trailing edge, and a circulation region fills downstream of the cavity, which is shown clearly in Figure 8(d). These findings are in agreement with Ravulapati et al. (2014), in which the shear layer interaction appeared near the corners. Figure 9 shows the vorticity contour in a cavity of the Reynolds number of 43471. These contours indicate the increasing the cavity distance also increases the vortex region which is consistent with Aradag et al. (2017). Figure 10 shows that at 10 mm of the vertical position (y/L), the peak velocity inside the cavity $U/U\infty$ is at P5, which is U/U = 0.86 m/s, followed by P4 ($U/U\infty$ = 0.75 m/s), P3($U/U\infty$ = 0.65 m/s), P2 ($U/U\infty$ = 0.60 m/s) and P1 ($U/U\infty$ = 0.26m/s). It shows that by increasing the cavity position, the velocity is also increased.

EFFECT OF REYNOLDS NUMBER

Figure 11 shows the velocity contour of different Reynolds number for cavity position at P5. The flow begins separated at Re = 17389 and produced a recirculation region called vortex inside the cavity. This recirculation region is also observed clearly at increasing the Reynold number (Re) of 26083, 34777 and 43471. Figure 12 shows that the low Reynolds number produces shear layer separation at the upstream leading edge and trailing edge. However, the two small corner vortices grow slightly in volume when reached Reynold number of 34777 and 43471. The results are due to the higher velocity produced thick flow separation shear layer that was created earlier at the upstream of the cavity. Therefore, these positions received substantial airflow compared with the first wind velocity. The velocity at the far location of P5 had increased. The velocity of the fluid flow inside the cavity increases as the Reynold number increases. Thus, this phenomenon showed that vortex flow influences the pressure and velocity inside the cavity.

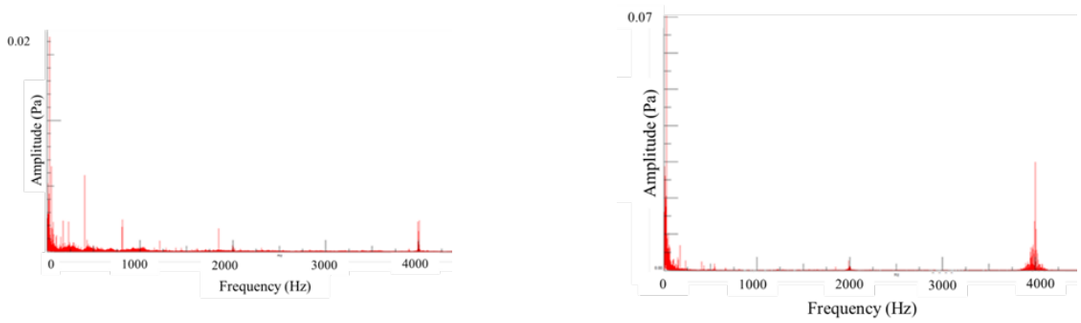

(a) (b)

FIGURE 6. (a) Background noise (b) Wind noise

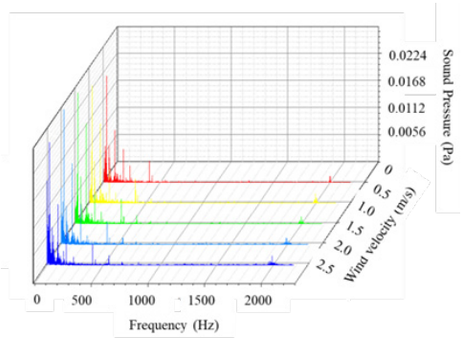

(a) P1

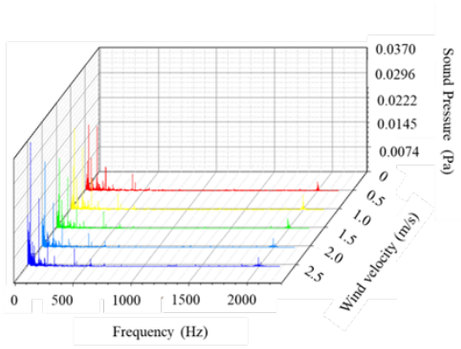

(b) P2

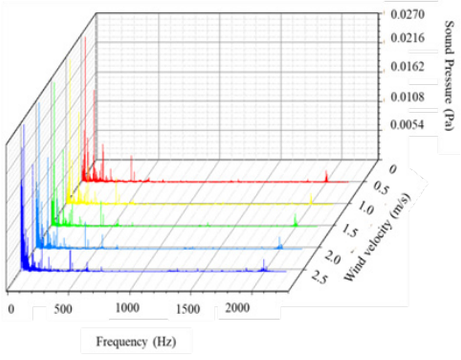

(c) P3

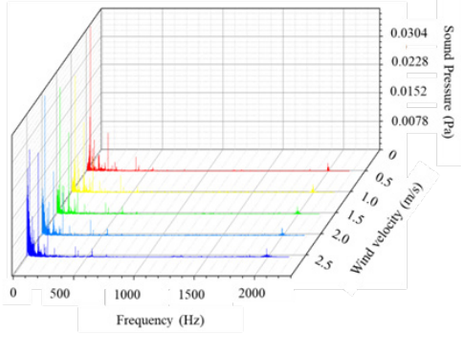

(d) P4

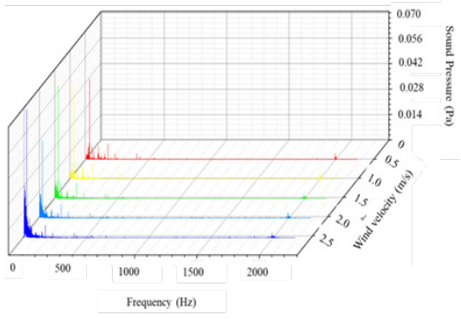

(e) P5

FIGURE 7. Sound pressure (Pa) against frequency (Hz) with varied cavity position and wind velocity

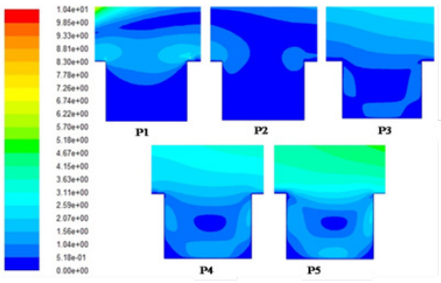

FIGURE 8. Velocity contour of different cavity position

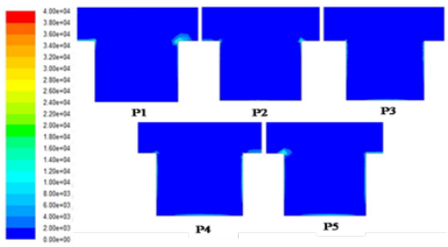

FIGURE 9. Vorticity magnitude of different cavity position

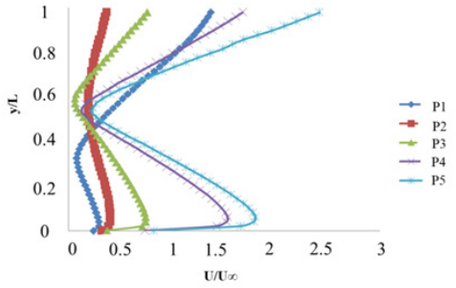

FIGURE 10. Comparison of velocity profile with different cavity position under Reynolds number of 43471.

TABLE 3. Velocity contour at the cavity floor at Reynolds number 43471

Cavity Position	Velocity (U/U∞)
P1	0.239
P2	0.326
P3	0.371
P4	0.740
P5	0.822

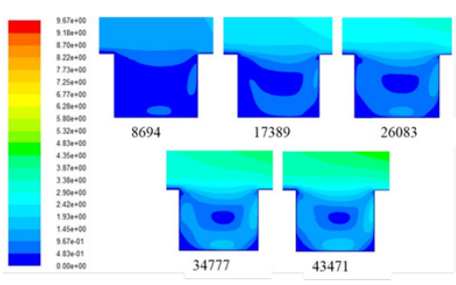

FIGURE 11. Velocity contour of different cavity position

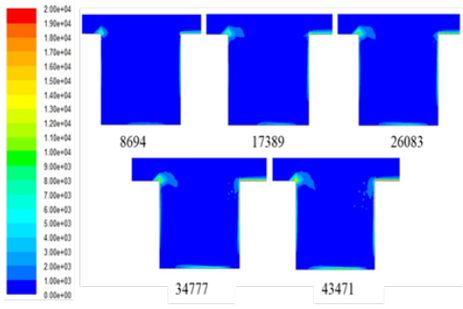

FIGURE 12. Vorticity magnitude contour of different cavity position

To reveal the cavity flow pattern inside the cavity at different Reynolds number, the vorticity magnitude contours for the case cavity position (P5) are shown in Figure 12. This figure shows the vortex shear layer interactions are observed at the leading edge, trailing edge and downstream of the cavity position (P5). This region is considered as the primary noise source (Koschatzky et al. 2011). The vorticity regions become weaker may be due to the lower wind speed or cavity is too close to the upstream corner. Even though the formation of vortex shedding is very weak, this vortex still causes a low-frequency wind-induced noise as stated by You et al. (2007), where the tip leakage vortex also causes a high noise level.

Figure 13 shows the comparison velocity profile at different Reynold numbers for cavity position (P5). The velocity inside the cavity increases with an increase in the Reynolds number. Overall, every curve has a similar variation.

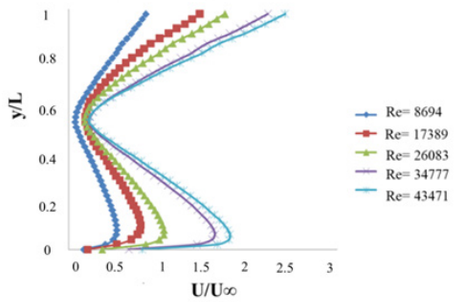

FIGURE 13. Comparison of velocity profile with different Reynolds numbers

TABLE 4. Velocity contour at the cavity floor at P5

Reynolds number	Velocity (U/U∞)
8694	0.168
17389	0.211
26083	0.375
34777	0.669
43471	0.822

CONCLUSION

This research studied SPL and flow structure behavior using wind tunnel test and CFD simulation at different parameters, such as cavity position and Reynolds number of the microphone cavity for two-way radios. The conclusion are as follows:

1. Wind tunnel test revealed that noise level increases with increasing wind velocity. However, noise level has only reached up to the maximum velocity at a particular cavity (i.e., P4). Noise level at cavity position P5 is reduced owing to the distant location from the wind noise. It shows that the cavity position of P5 is a suitable distance to reduce the wind noise.
2. The evolution of vortices inside the cavity appeared clearly from Re = 26083 to Re = 43471. Accordingly, the vortex increases when the Reynolds number increases.

ACKNOWLEDGEMENT

The authors would like to thank Universiti Sains Malaysia (USM) for their financial support under the CREST Grant No. (304/PMEKANIK/6050242) and RUI grant (Grant No. 001/PAERO/8014005).

DECLARATION OF COMPETING INTEREST

None.

REFERENCES

Aradag, S., Gelisli, K. A., & Yaldir, E. C. 2017. Effects of active and passive control techniques on mach 1.5 cavity flow dynamics. *International Journal of Aerospace Engineering*.

Das, R., and Kurian. 2013 Acoustic and velocity field over 3D cavities. *Theoretical & Applied Mechanics Letters* 3, 012001.

Fisol, Ummi Masyitah Mohd, et al. "Wind noise analysis of two-way radio." *Smart Instrumentation, Measurement Applications (ICSIMA), 2013 IEEE International Conference on*. IEEE, 2013.

Hairudin, W. M., Ismail, N. A., & Ripin, Z. M. 2020. Simulation of flow distribution inside small cavity at two-way radio by CFD (Ansys Fluent). In *Advancement in Emerging Technologies and Engineering Applications* (pp. 393-398). Singapore: Springer, Singapore.

Hashim, M.K.R., Ismail, N.A., Saad, A.A., Chan, P.Y., Fisol, U.M.M., Ripin, Z.M., Yow, H.T., Tan, C.H., Hii, U.H. and Saw, T.S., 2013, November. Sound quality analysis for two-way radio under wind noise. In *Smart Instrumentation, Measurement and Applications (ICSIMA), 2013 IEEE International Conference on* (pp. 1-5)

Kook, H., & Mongeau, L. 2002. Analysis of the periodic pressure fluctuations induced by flow over a cavity. *Journal of Sound and Vibration* 251(5): 823-846.

Koschatzky, V., Moore, P. D., Westerweel, J., Scarano, F., & Boersma, B. J. 2011. High speed PIV applied to aerodynamic noise investigation. *Experiments in Fluids* 50(4): 863-876.

Liu, J. 2012. Simulation of whistle noise using computational fluid dynamics and acoustic finite element simulation. Master Thesis, Lexington, University of Kentucky.

Mishra, P., & Aharwal, K. R. 2018. A review on a selection of turbulence model for CFD analysis of airflow within cold storage. In *IOP Conference Series: Materials Science and Engineering* (Vol. 402, No. 1, p. 012145). IOP Publishing.

Morgan, S., & Raspet, R. 1992. Investigation of the mechanisms of low-frequency wind noise generation outdoors. *The Journal of the Acoustical Society of America* 92(2): 1180-1183.

Proskurov, S. 2017. Aerofoil broadband and tonal noise modelling using Fast-Random-Particle-Mesh method and Large Eddy *Simulation* (Doctoral dissertation, Queen Mary University of London).

Ravulapati, K. 2014. *Separation Bubbles and Vortex Formation in Cavity Flows*. Embry riddle Aeronautical Universit.

Saw, T. S., Tan, C. H., & Yow, H. T. 2018. *U.S. Patent No. 9,877,097*. Washington, DC: U.S. Patent and Trademark Office.

Sridhar, V., Gai, S. L., & Kleine, H. (2012, December). A Numerical Investigation of Supersonic Cavity Flow at Mach 2. In *18th Australasian Fluid Mechanics Conference, Launceston, Australia*.

Yow, Huoy Thyng, et al. 2013. Prediction of wind-induced noise over bodies and small cavity. *The Journal of the Acoustical Society of America* 134(5): 4222-4222.

You, D., Wang, M., Moin, P. and Mittal, R. 2007. Vortex dynamics and low-pressure fluctuations in the tip-clearance flow. *Journal of Fluids Engineering* 129(8): 1002-1014.

Zhang, N., Shen, H. C., & Yao, H. Z. 2010. Numerical simulation of cavity flow-induced noise by LES and FW-H acoustic analogy. *Journal of Hydrodynamics, Ser. B* 22(5): 242-247.

Zhao, S., Cheng, E., Qiu, X., Burnett, I., & Liu, J. C. C. 2017. Wind noise spectra in small Reynolds number turbulent flows. *The Journal of the Acoustical Society of America* 142(5): 3227-3233.

Zhao, S., Dabin, M., Cheng, E., Qiu, X., Burnett, I., & Liu, J. C. C. 2018. Mitigating wind noise with a spherical microphone array. *The Journal of the Acoustical Society of America* 144(6): 3211-3220.

Wang, L, Zander, AC & Lenchine, VV 2012. 'Measurement of the Self-Noise of Microphone Wind Shields', 18th Australasian Fluid Mechanics Conference, Launceston, Australia.

Pascioni, K., Reger, R., Edstrand, A., & Cattafesta, L. 2014. Characterization of an aeroacoustic wind tunnel facility. In *INTER-NOISE and NOISE-CON Congress and Conference Proceedings* (Vol. 249, No. 3, pp. 3966-3975). Institute of Noise Control Engineering.